

# Superior Efficacy and Selectivity of Novel Small-Molecule Kinase Inhibitors of T790M-Mutant EGFR in Preclinical Models of Lung Cancer

Jin Kyung Rho<sup>1,2,3</sup>, In Yong Lee<sup>4</sup>, Yun Jung Choi<sup>1,3</sup>, Chang-Min Choi<sup>3,5</sup>, Jae-Young Hur<sup>1,3</sup>, Jong Sung Koh<sup>4</sup>, Jaekyoo Lee<sup>4</sup>, Byung-Chul Suh<sup>4</sup>, Ho-Juhn Song<sup>4</sup>, Paresh Salgaonkar<sup>4</sup>, Jungmi Lee<sup>4</sup>, Jaesang Lee<sup>6</sup>, Dong Sik Jung<sup>6</sup>, Sang-Yeob Kim<sup>1,2</sup>, Dong-Cheol Woo<sup>1,2</sup>, In-Jeoung Baek<sup>1,2</sup>, Joo-Yong Lee<sup>1,2</sup>, Chang Hoon Ha<sup>1,2</sup>, Young Hoon Sung<sup>1,2</sup>, Jeong Kon Kim<sup>7</sup>, Woo Sung Kim<sup>3</sup>, Joon Seon Song<sup>8</sup>, Cheol Hyeon Kim<sup>9</sup>, Trevor G. Bivona<sup>10,11</sup>, and Jae Cheol Lee<sup>5</sup>

## Abstract

The clinical utility of approved EGFR small-molecule kinase inhibitors is plagued both by toxicity against wild-type EGFR and by metastatic progression in the central nervous system, a disease sanctuary site. Here, we report the discovery and preclinical efficacy of GNS-1486 and GNS-1481, two novel small-molecule EGFR kinase inhibitors that are selective for T790M-mutant isoforms of EGFR. Both agents were effective in multiple mouse xenograft models of human lung adenocarcinoma (T790M-positive or -negative), exhibiting less activity against wild-type EGFR than existing approved EGFR kinase inhibitors (including osimertinib). In addition, GNS-1486 showed superior potency against intracranial metastasis of EGFR-mutant lung adenocarcinoma. Our results offer a preclinical proof of concept for new EGFR kinase inhibitors with the potential to improve therapeutic index and efficacy against brain metastases in patients. *Cancer Res*; 77(5); 1200–11. ©2017 AACR.

precision cancer medicine with great promise for improving patient survival and quality of life (3, 4–10). However, in the case of EGFR-mutant lung adenocarcinoma, both clinical toxicity due to residual activity against wild-type (WT) EGFR versus mutant EGFR and metastatic tumor progression in the central nervous system (CNS) are two remaining obstacles that limit the overall clinical impact of the current first- (gefitinib, erlotinib), second- (afatinib), and third-generation (osimertinib) EGFR tyrosine kinase inhibitors (TKI) that are FDA approved (11, 12, 13–18, 19). Importantly, lung adenocarcinoma patients with CNS metastasis have a particularly dismal prognosis, as no drug therapy has shown consistent or durable efficacy against intracranial metastasis to date (19, 20).

## Introduction

Lung cancer is the leading cause of cancer mortality worldwide, with lung adenocarcinoma as the most common histologic subtype (1, 2). The clinical success of oncogene-targeted therapy in specific subsets of lung adenocarcinoma patients, such as those with activating mutations in EGFR, has heralded a new era of

During the treatment of EGFR-mutant lung adenocarcinoma patients with first-generation EGFR TKIs (erlotinib, gefitinib), tumor progression often occurs via the emergence of the EGFR<sup>T790M</sup> resistance mutation (21, 22). This observation prompted the development of second- and third-generation irreversible EGFR inhibitors with activity against EGFR<sup>T790M</sup> (21, 23, 24). Some of these newer EGFR inhibitors, such as CO-1686 (rociletinib) and AZD9291 (osimertinib), exhibit increased selectivity for mutant EGFR with relative sparing of WT EGFR, as compared with earlier EGFR inhibitors, including erlotinib, gefitinib, and afatinib (12). This relative selectivity for mutant EGFR over WT EGFR can enhance the therapeutic index for EGFR inhibition in patients, potentially reducing certain toxicities that occur because of WT EGFR blockade (such as cutaneous and gastrointestinal side effects; refs. 25, 26). Although the development of CO-1686 (rociletinib) has been discontinued (in part due to less impressive clinical efficacy than initially anticipated), AZD9291 (osimertinib) is now approved for the

<sup>1</sup>Asan Institute for Life Sciences, Asan Medical Center, College of Medicine, University of Ulsan, Seoul, Korea. <sup>2</sup>Department of Convergence Medicine, Asan Medical Center, College of Medicine, University of Ulsan, Seoul, Korea. <sup>3</sup>Department of Pulmonology and Critical Care Medicine, Asan Medical Center, College of Medicine, University of Ulsan, Seoul, Korea. <sup>4</sup>Genosco, Cambridge, Massachusetts. <sup>5</sup>Department of Oncology, Asan Medical Center, College of Medicine, University of Ulsan, Seoul, Korea. <sup>6</sup>Oscotec Inc., Seongnam, Korea. <sup>7</sup>Department of Radiology, Research Institute of Radiology, Asan Medical Center, College of Medicine, University of Ulsan, Seoul, Korea. <sup>8</sup>Department of Pathology, Asan Medical Center, College of Medicine, University of Ulsan, Seoul, Korea. <sup>9</sup>Department of Internal Medicine, Korea Cancer Center Hospital, Seoul, Korea. <sup>10</sup>Department of Medicine, University of California San Francisco, San Francisco, California. <sup>11</sup>Helen Diller Family Comprehensive Cancer Center, University of California San Francisco, San Francisco, California.

**Note:** Supplementary data for this article are available at Cancer Research Online (<http://cancerres.aacrjournals.org/>).

J.K. Rho and I.Y. Lee contributed equally to this article.

**Corresponding Authors:** Trevor G. Bivona, Helen Diller Family Comprehensive Cancer Center, University of California, San Francisco, 600 16th Street, N212D, San Francisco, CA 94158. Phone: 415-476-9907; Fax: 415-514-0169; E-mail: trever.bivona@ucsf.edu; Jin Kyung Rho, jkrho@amc.seoul.kr; and Jae Cheol Lee, jcllee@amc.seoul.kr

**doi:** 10.1158/0008-5472.CAN-16-2432

©2017 American Association for Cancer Research.

second-line treatment of lung adenocarcinoma patients with EGFR<sup>T790M</sup>-positive disease (25, 26). Although osimertinib appears to be associated with decreased clinical toxicity (by historical comparison with first- and second-generation EGFR TKIs), side effects linked to residual activity against WT EGFR remain a clinical challenge and impair the quality of life in patients (including grade 3 adverse events occurring in ~33% of osimertinib-treated individuals; toxicity that is consistent with the experience using osimertinib in our own clinical practices; 25–28). In addition to the clinical toxicity and quality-of-life issues, the recommended drug dose (or in some cases dose reduction or suspension) that is used as a consequence of the toxicity resulting from the submaximal selectivity for mutant EGFR over WT EGFR of the current FDA-approved EGFR TKIs can lead to incomplete (or nonsustained) target inhibition in both intracranial and extracranial tumor cells, thereby potentially contributing to the progression of metastatic tumors both within and outside of the CNS (11, 21, 26, 29).

Disease progression in the CNS, a sanctuary site, is a widespread cause of death in EGFR-mutant lung adenocarcinoma patients (19). Limited published reports show that the current approved EGFR inhibitors (including osimertinib) have documented but inconsistent and often temporary clinical efficacy against CNS metastases [abstracts: Kim D and colleagues *Annals of Oncology* (2014) 25 (Suppl\_4): iv146-iv164. 10.1093/annonc/mdl331; Camidge DR and colleagues *MINI16.04*, 16th World Conference on Lung Cancer, 2015; Sequist LV and colleagues *J Clin Oncol*. 2014;32 (15 Suppl): abstract 8010 2014 ASCO Annual Meeting; refs. 7, 19, 24, 25, 26, 30, 31]. There remains no established and widely effective systemic treatment for CNS metastases in patients with EGFR-mutant lung adenocarcinoma, and progression of CNS metastasis has been reported and observed in our own clinical practices in patients treated with all current FDA-approved EGFR inhibitors, including osimertinib (Ahn MJ, and colleagues *ESMO 2015*. Abstract 3083; refs. 19, 28, 32). Thus, although recently initiated clinical trials are testing certain EGFR TKIs, such as osimertinib, in patients with CNS metastasis (e.g., NCT02736513), the CNS antitumor efficacy of the EGFR TKIs that are currently approved remains an unresolved and active area of investigation.

To address the limitations of the current approved EGFR TKIs, we conducted a drug discovery program to discover a potent, mutant-selective EGFR TKI with less WT EGFR activity and thus potentially a wider therapeutic index versus the currently approved EGFR TKIs and that also exhibits pronounced activity against intracranial EGFR-mutant lung adenocarcinoma metastasis. This discovery program has led to the identification of two novel and improved EGFR TKIs; the data provide the rationale for clinical trials that will be initiated soon testing these promising new agents in EGFR-mutant (including EGFR<sup>T790M</sup>) lung adenocarcinoma patients with intracranial and extracranial metastatic disease.

## Materials and Methods

### Cell culture and reagents

The human non-small cell lung cancer (NSCLC) cell lines (HCC827 and H1975) and NIH 3T3 (mouse embryonic fibroblast cell line) were obtained from the ATCC. PC-9 cells were a gift from F. Koizumi and K. Nishio (National Cancer Center Hospital, Tokyo, Japan). PC-9/GR (gefitinib-resistant cell line) and PC-9/ER

(erlotinib-resistant cell line) cells were established as part of a previous study (33). Cells were cultured in RPMI1640 medium containing 10% FBS, 2 mmol/L L-glutamine, and 100 U/mL of penicillin and streptomycin, and maintained at 37°C in a humidified chamber containing 5% CO<sub>2</sub>. Osimertinib, CO-1686, and WZ4002 were purchased from Selleck Chemicals. The cell lines used were authenticated by STR analysis and confirmed to be mycoplasma free using standard methods.

### Cellular viability assays

To perform the MTT assay, cells ( $5 \times 10^3$ ) were seeded in 96-well sterile plastic plates overnight and then treated with relevant agents. After 72 hours, 15  $\mu$ L of MTT solution (5 mg/mL) was added to each well, and plates were incubated for 4 hours. Crystalline formazan was solubilized with 100  $\mu$ L of a 10% (w/v) SDS solution for 24 hours, and then absorbance at 595 nm was read spectrophotometrically using a microplate reader. To test the colony formation assay, cells ( $0.1-1 \times 10^3$ ) were seeded in 6-well plates and then treated with relevant agents. After 10 to 14 days, the colonies were stained with crystal violet and counted. The results are representative of at least three independent experiments, and the error bars signify SDs.

### Cell-free kinase assay

Cell-free kinase assays were conducted using Lance Ultra time-resolved fluorescence resonance energy transfer technology according to the manufacturer's instructions (PerkinElmer). Briefly, various concentrations of EGFR inhibitors were mixed with each enzyme (WT or mutant EGFR, Her2, and Her4), the Ulight-poly-GT peptide substrate and ATP in a kinase buffer (50 mmol/L HEPES pH 7.5, 10 mmol/L MgCl<sub>2</sub>, 1 mmol/L EFTA, 2 mmol/L DTT, and 0.01% Tween-20) in a 96-well plate. Kinase reactions were incubated at room temperature for 1 hour and then stopped by the addition of EDTA. The specific europium-labeled anti-phospho peptide antibody (PerkinElmer) was added to the reaction in Lance detection buffer. The mixture was allowed to incubate for 30 minutes to allow binding of the antibody to the phosphorylated site before the plate was read. The LANCE signal was measured on an EnVision Multilabel Reader (PerkinElmer). Excitation wavelength was set at 320 nm, and emission was monitored at 615 nm (donor) and 665 nm (acceptor). The IC<sub>50</sub> values were determined using GraphPad Prism software.

### Kinase profile assay

The kinase selectivity was assessed by KinaseProfiler (Millipore) consisting of 321 kinases for GNS-1481 or 323 kinases for GNS-1486 and osimertinib at a single concentration of 1  $\mu$ mol/L using ATP  $K_m$  for each kinase.

### Expression vectors and transfections

EGFR constructs (EGFR wild-type, EGFR del746-750, EGFR T790M/L858R, and EGFR T790M/del746-750) were purchased from Addgene. Transfections were performed using Lipofectamine 2000 (Invitrogen) in accordance with the manufacturer's instructions. Transfected cells were selected using puromycin (2  $\mu$ g/mL for NIH3T3; Sigma).

### Immunoblotting

Cells were lysed in buffer containing 137 mmol/L NaCl, 15 mmol/L EGTA, 0.1 mmol/L sodium orthovanadate, 15 mmol/L MgCl<sub>2</sub>, 0.1% Triton X-100, 25 mmol/L MOPS, 100 mmol/L phenylmethylsulfonyl fluoride, and 20 mmol/L leupeptin,

Rho et al.

adjusted to pH 7.2. Lysis of tumor specimens was performed using Omni Tissue Homogenizer (TH; Omni International). Antibodies specific for p-EGFR (Tyr1173), EGFR, Akt, ERK, and actin were obtained from Santa Cruz Biotechnology, and antibodies for PARP, caspase 3, p-Akt (Ser473), and p-ERK (Thr202/Tyr204) were purchased from Cell Signaling Technology. Proteins were detected with an enhanced chemiluminescence Western Blotting Kit (Amersham Biosciences), according to the manufacturer's instructions.

#### Animal models

To establish xenograft models, female SCID mice (18–20 g, 6 weeks of age) were purchased from Charles River Laboratories. All experimental procedures were conducted following a protocol approved by the Institutional Animal Care and Use committee of Asan Institute for Life Sciences (Seoul, Korea; 2014-12-103 and 2015-12-087). Tumors were grown by implanting cells ( $1-5 \times 10^6$  cells/0.1 mL) in 50% Matrigel (BD Biosciences) and subcutaneously injected into the right flank of animals. Drug treatment was started when the tumors reached a volume of 50 to 100 mm<sup>3</sup>. To measure tumor size, the length (*L*) and width (*W*) of each tumor was measured using calipers, and tumor volume (TV) was calculated as  $TV = (L \times W^2)/2$ . To perform the intracranial implantation of HCC827-luc cells, the human NSCLC cell line HCC827 was stably integrated with a luciferase reporter gene, RediFect lentiviral particles (PerkinElmer). Female athymic nude mice (6–8 weeks of age, Charles River Laboratories) were anesthetized with a ketamine/xylazine cocktail solution. The head of the mouse was stabilized by using a Harvard Apparatus stereotaxic head frame. After disinfection of the skin, a 1-cm midline scalp incision was made, and a burr hole (coordinates, 2.5 mm lateral and 0.5 mm posterior to the bregma) in the skull was made by using a high-speed microdrill. Cells ( $1-5 \times 10^5$  cells/4  $\mu$ L serum-free RPMI) were injected into the right striatum using a 10  $\mu$ L Hamilton syringe to deliver tumor cells to a 3.5-mm intraparenchymal depth. The burr hole in the skull was sealed with bone wax and the incision closed using Dermabond. Tumor growth was monitored and measured via bioluminescence imaging (BLI) *in vivo*.

#### Drug administration

GNS-1481 and -1486 were dissolved in NMP/PEG300 (1:9, v/v), and osimertinib and CO-1686 were dissolved in Tween-80. All drugs were given by oral intubation for the indicated times.

#### Bioluminescence monitoring and $\mu$ CT coregistration of intracranial tumors

Intracranial tumor growth quantified by BLI was performed using an IVIS spectrum system (Caliper, PerkinElmer Company). Mice were administered by intraperitoneal injection with 150 mg/kg body weight of D-luciferin (Caliper Life Sciences) dissolved in DPBS (Gibco). Before and during imaging, mice were anesthetized by 1% isoflurane inhalation (Forane). Bioluminescent signals were acquired with open filter or emission at 620 nm using autoacquisition and field of view of 13.4 cm, and bioluminescent signals were quantified as radiance (photon/sec/cm<sup>2</sup>/sr) within a circular region of interest (ROI) using Living Image 4.4 software. To visualize the anatomic location, mice were imaged with a Quantum FX  $\mu$ CT system after optical imaging.  $\mu$ CT image used a 120 mm FOV with a 236  $\mu$ m voxel

size and a dose of 26 mGy per scan. Three-dimensional (3D) optical and reconstructed  $\mu$ CT images were automatically generated with the Living Image 4.4 Software and 3D ROIs were measured as voxels (photons/second).

#### Immunohistochemical staining

Each tumor was harvested at the indicated times postadministration with drugs. Resected tumors were fixed in 10% formaldehyde and embedded in paraffin. Immunohistochemical staining was done using a specific primary antibody (Ki-67; DakoCytomation), the EnVision Plus Staining Kit (DakoCytomation), and APO-Direct terminal deoxynucleotidyl transferase-mediated dUTP nick end labeling (TUNEL) Assay Kit (Millipore) according to the supplier's instructions. Quantitative analysis of section staining was done by counting immunopositive cells in five arbitrarily selected fields.

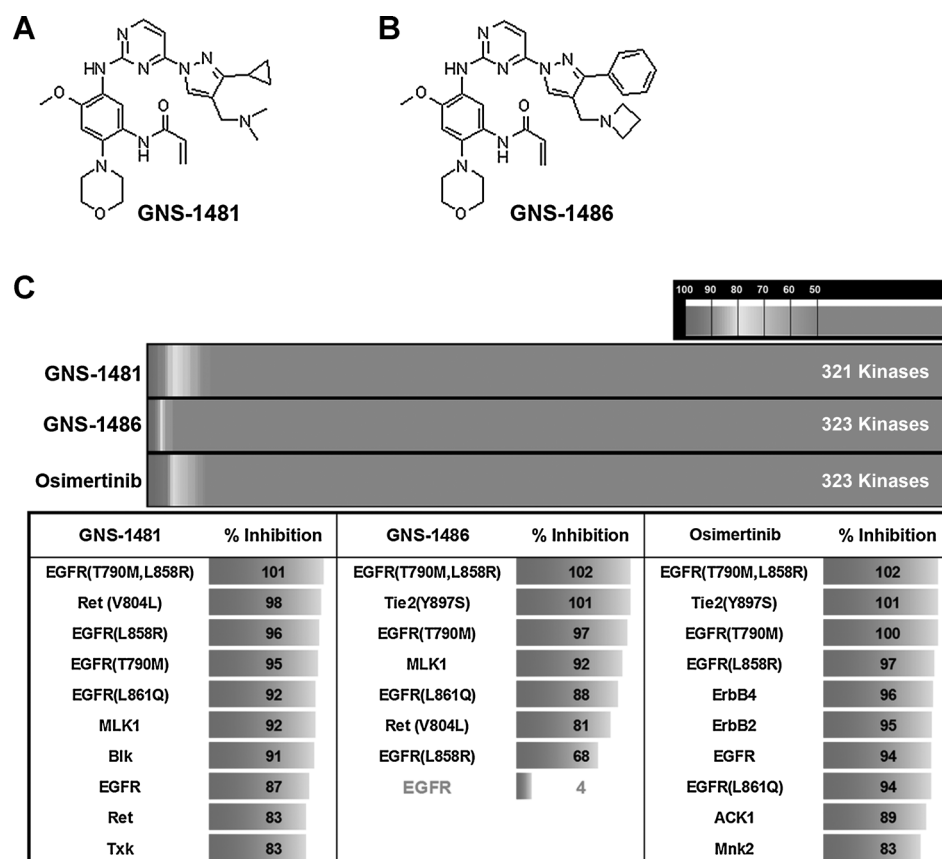
#### Statistical analysis

*P* values were determined with unpaired *t* tests between comparator groups using GraphPad software.

## Results

#### Discovery and characterization of novel mutant-selective EGFR TKIs

In search of novel WT or mutant EGFR (Del 19, E746-A750), L858R, L858R/T790M, T790M, Del 19/T790M) inhibitors, we performed a high-throughput screen of a proprietary compound library consisting of 1,583 structurally diverse molecules. This campaign led to the identification of 30 compounds displaying activity against mutant EGFR. Structure-based drug design utilizing structure activity relationship information from the 30 hit compounds led to several potent and selective inhibitors with favorable physical properties and *in vitro* ADME (absorption, distribution, metabolism, and excretion). Among those 30 compounds, two novel 3-pyrazolopyrimidine compounds (GNS-1481 and GNS-1486) were identified as potent and selective irreversible EGFR inhibitors against all forms of mutant EGFR tested. GNS-1481 and GNS-1486 contain a pyrimidine-based scaffold, analogous to other third-generation EGFR kinase inhibitors (Fig. 1A and B; refs. 23, 24). GNS-1481 and GNS-1486 exhibited broad activity at low nanomolar concentrations against all EGFR mutations tested, including EGFR<sup>T790M</sup> in kinase inhibition *in vitro* assays (Table 1). Moreover, GNS-1481 and GNS-1486 showed substantial selectivity for mutant EGFR as compared with WT EGFR, as indicated by the selectivity index (defined as the ratio of the IC<sub>50</sub> for WT EGFR/IC<sub>50</sub> for the L858R-T790M double mutant, Table 1, bottom row). GNS-1486, in particular, showed superior selectivity for mutant EGFR over WT EGFR compared with the other approved EGFR inhibitors, including osimertinib (Table 1). Structural modeling studies of the thermodynamics and binding of GNS-1481 and GNS-1486 to either WT or mutant EGFR suggested distinct interactions enabling a tighter association with mutant EGFR versus WT EGFR overall and improved mutant selectivity compared with osimertinib in general, consistent with the kinase profiling studies (Supplementary Fig. S1; Table 1). These findings indicating the substantial potency and mutant EGFR selectivity of the GNS compounds were further extended across a panel of approximately 320 kinases in a multikinase inhibition assay *in vitro* (Fig. 1C; Supplementary Table S1). Although strong activity against



various forms of mutant EGFR was observed for GNS-1481 and GNS-1486 (each tested at 1 μmol/L), these agents exhibited less or minimal activity against WT EGFR or other EGFR family members, such as ErbB2 and ErbB4, when compared with osimertinib (Fig. 1C; Supplementary Table S1). Interestingly, we noted that GNS-1481 and GNS-1486, in contrast to osimertinib, exhibited *in vitro* activity against RET [either WT or the gatekeeper mutant V804L that is resistant to certain other RET inhibitors (34)], an oncogene in other tumor types including thyroid cancer and a distinct subset of lung adenocarcinoma driven by RET gene rearrangements (Fig. 1C; Supplementary Table S1; refs. 34, 35). Furthermore, GNS-1481 and GNS-1486 showed unique activity against MLK1 (mixed-lineage kinase 1), which can activate MEK-ERK signaling and promote RAF inhibitor resistance in melanoma (Fig. 1C; Supplementary Table S1; ref. 36). Together, these biochemical data reveal the

high potency, substantial mutant EGFR selectivity, and unique target profiles of the two novel irreversible EGFR inhibitors we identified, GNS-1481 and GNS-1486.

#### Preclinical efficacy of the novel mutant-selective EGFR kinase inhibitors GNS-1481 and GNS-1486 *in vitro*

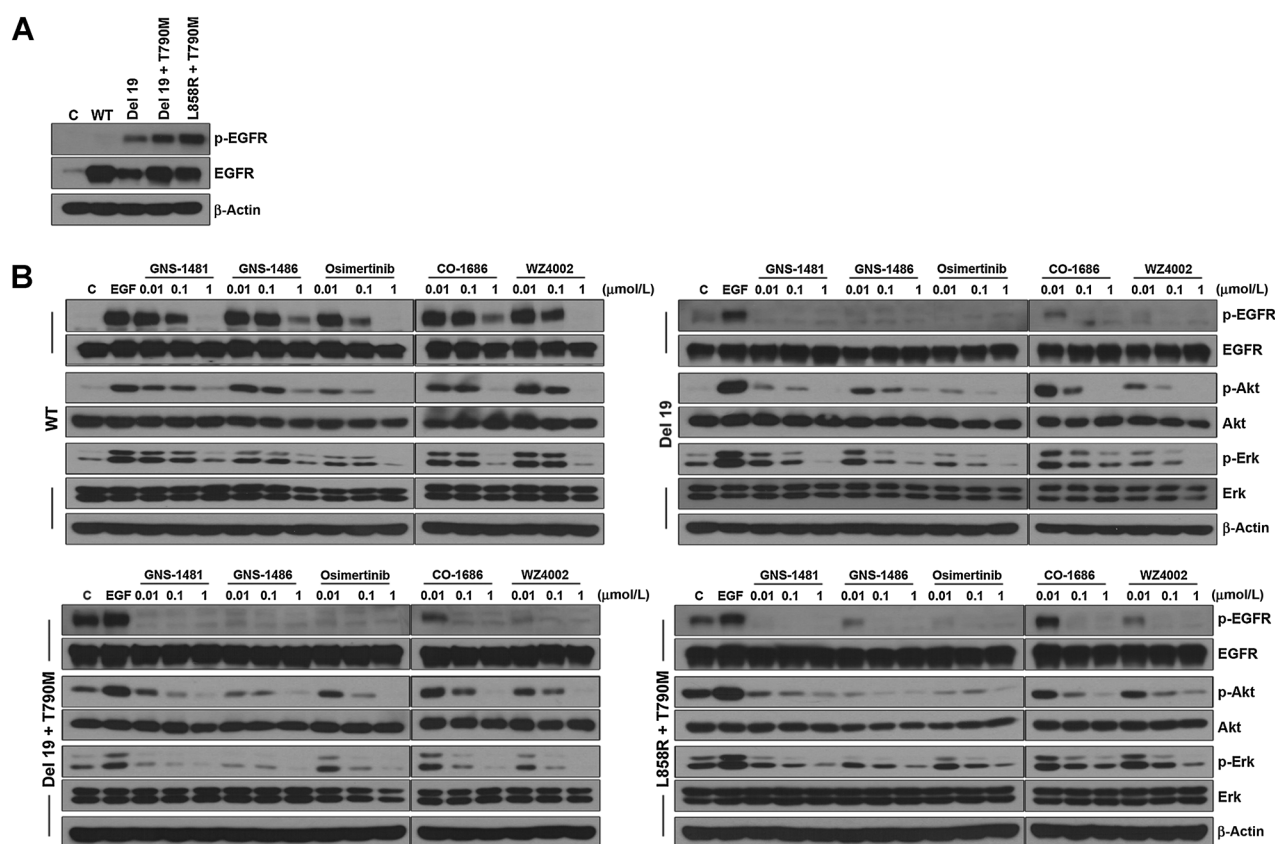
We next examined the activity of both GNS-1481 and GNS-1486 on signaling and cell viability in EGFR-mutant preclinical models. We first studied the impact of treatment with each agent and with other third-generation EGFR inhibitors (osimertinib, CO-1686, and WZ4002; ref. 37) on signaling in NIH-3T3 cells engineered to express either WT or mutant EGFR (Del 19, Del 19/T790M, L858R/T790M; Fig. 2A and B). GNS-1481 and GNS-1486 had comparatively minimal impact on the levels of phosphorylated (p)-EGFR, or the downstream signaling components p-ERK and p-AKT, in WT EGFR-expressing cells, consistent with the WT

**Table 1.** Multikinase inhibition profiles for GNS-1481 and GNS-1486, and the other indicated EGFR kinase inhibitors

| Kinase                                | GNS-1481 | GNS-1486 | Osimertinib | CO-1686 | Afatinib | Erlotinib |
|---------------------------------------|----------|----------|-------------|---------|----------|-----------|
| EGFR                                  |          |          |             |         |          |           |
| Wild type                             | 26.5     | 121.6    | 16.7        | 928.2   | 0.2      | 0.6       |
| Del19 (E746-A750)                     | 6.6      | 20.5     | 8.6         | 216.5   | 0.2      | 0.8       |
| L858R                                 | 25.8     | 103.6    | 12.2        | 742.9   | 0.3      | 0.9       |
| Double mutant (L858R-T790M)           | 6.2      | 8.3      | 4.5         | 45.7    | 18.6     | 549.3     |
| T790M                                 | 3.4      | 4.2      | 2.2         | 20.5    | 1.6      | 395.2     |
| Double mutant (Del19-T790M)           | 4.2      | 4.3      | 3.3         | 44.1    | 7.0      | 715.6     |
| Wild type/double mutant (L858R-T790M) | 4.3      | 14.7     | 3.7         | 20.3    | 0.01     | <0.01     |

NOTE: Shown is the IC<sub>50</sub> in nmol/L of each drug against the kinase activity of each indicated protein. The bottom row indicates the mutant-selective index (increased proportional to the degree of mutant-selective activity, ratio calculated as the IC<sub>50</sub> WT EGFR/L858R-T790M double mutant).

Rho et al.

**Figure 2.**

Preclinical efficacy of the novel mutant-selective EGFR kinase inhibitors GNS-1481 and GNS-1486 *in vitro*. **A** and **B**, Effects of treatment with the indicated EGFR kinase inhibitors on the indicated signaling components in the indicated NIH-3T3 cell lines engineered to stably express either WT EGFR or each form of mutant EGFR shown. Effects of treatment with the indicated EGFR kinase inhibitors (for 5 hours) on the indicated signaling components are shown. Results represent at least three independent experiments.

EGFR-sparing activity of these agents observed in the biochemical assays (Fig. 2B; Supplementary Fig. S2A). In contrast, treatment with each agent suppressed the levels of p-EGFR, p-ERK, and p-AKT and induced cleavage of PARP (as a measure of apoptosis) in each EGFR-mutant model (Fig. 2A and B; Supplementary Fig. S2A and B). We did not find substantial *in vitro* activity of the GNS agents against the C797S-mutant form of EGFR that can promote resistance to other third-generation EGFR inhibitors, such as osimertinib (data not shown; ref. 27).

We next assessed the effects of GNS-1481 and GNS-1486 treatment on cell viability in human EGFR-mutant lung adenocarcinoma cell lines, including those with EGFR<sup>T790M</sup>. We found that treatment with either agent was highly effective against multiple EGFR-mutant models *in vitro* (including PC9 and HCC827 cells with Del 19; Fig. 3A and B; Supplementary Table S2). Moreover, GNS-1481 and GNS-1486 exhibited substantial efficacy in EGFR<sup>T790M</sup>-positive lung adenocarcinoma models *in vitro*, including PC-9/GR and PC-9/ER sublines with acquired resistance to gefitinib or erlotinib (33, 38), respectively, and H1975 cells that intrinsically harbor EGFR<sup>L858R/T790M</sup> (Fig. 3A and B; Supplementary Table S2). We further established the specificity of GNS-1481 and GNS-1486 efficacy for lung cancer cells with mutant EGFR by testing these agents in multiple EGFR WT lung cancer models, including A549, H460, and A341 cells.

We found no significant impact of treatment with either agent on cell viability in these models (Supplementary Fig. S2C). GNS-1481 and GNS-1486 (or osimertinib) monotherapy had no significant effect on the viability of EGFR-mutant lung adenocarcinoma cells with acquired erlotinib/gefitinib resistance driven by non-EGFR<sup>T790M</sup>-mediated mechanisms, such as MET and AXL kinase upregulation, as expected (Supplementary Fig. S2D; refs. 39, 40). Together, these findings further establish the substantial and specific activity of GNS-1481 and GNS-1486 in multiple EGFR<sup>T790M</sup> (–) and (+) EGFR-mutant lung adenocarcinoma preclinical models.

Analysis of the impact of GNS-1481 and GNS-1486 treatment on key signaling components in the EGFR-mutant lung adenocarcinoma models (PC-9, PC-9/GR, PC-9/ER, and H1975) revealed that each agent suppressed the levels of p-EGFR, p-ERK, and p-AKT in each system (Fig. 3C; Supplementary Fig. S2E). Treatment with GNS-1481 and GNS-1486 was lethal in these EGFR-mutant lung adenocarcinoma cell lines, as these effects on signaling were accompanied by the induction of apoptosis upon GNS-1481 and GNS-1486 treatment, indicated by increased levels of both cleaved PARP and caspase-3 (Supplementary Fig. S2F). Together, these data indicate that GNS-1481 and GNS-1486 are novel mutant-selective EGFR inhibitors that strongly suppress mutant EGFR signaling and induce apoptosis, resulting in

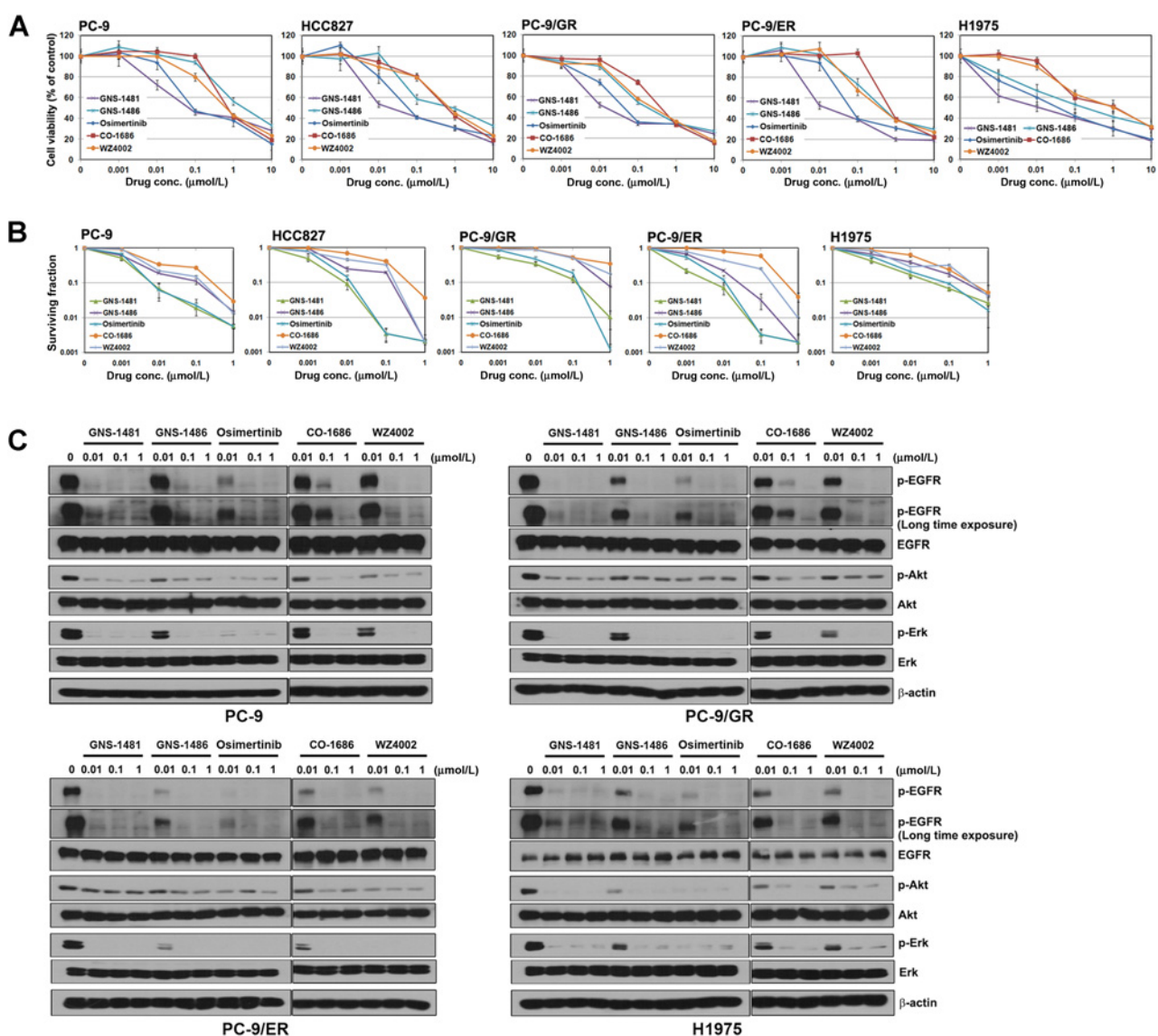


**Figure 3.**

Preclinical efficacy of the novel mutant-selective EGFR kinase inhibitors GNS-1481 and GNS-1486 *in vitro* in lung cancer models. **A** and **B**, Effects of treatment with the indicated EGFR kinase inhibitors on cell viability in the indicated human lung adenocarcinoma cell lines with endogenous mutant EGFR ( $n = 3$ ,  $\pm$ SEM). The sensitivity to EGFR inhibitor treatment was determined by MTT assay (**A**) and colony formation assay (**B**). **C**, Effects of treatment with the indicated EGFR kinase inhibitors (for 5 hours) on the indicated signaling components in the cell lines in **A** and **B**. Results represent at least three independent experiments.

substantial efficacy in multiple EGFR<sup>T790M</sup> (–) and (+) EGFR-mutant lung adenocarcinoma preclinical models. Overall, we noted in these *in vitro* studies that the GNS agents showed superior WT EGFR-sparing properties compared with the other clinically approved EGFR TKIs and demonstrated therapeutic effects that are comparable with the other third-generation EGFR inhibitors tested (with relatively subtle differences observed across these *in vitro* systems and the parameters measured).

#### Preclinical efficacy of the novel mutant-selective EGFR kinase inhibitors GNS-1481 and GNS-1486 *in vivo*

Supported by our encouraging findings showing improved sparing of WT EGFR, substantial mutant EGFR-selective potency,

and efficacy *in vitro*, we next investigated the *in vivo* properties of GNS-1481 and GNS-1486, including pharmacokinetic, pharmacodynamic, safety, and antitumor efficacy analysis. *In vivo* pharmacology and pharmacokinetic studies in mouse, rat, and dog revealed substantial exposure upon oral administration at 10 mg/kg for mouse and rat and 5 mg/kg for dog (Supplementary Fig. S3A, data not shown). This oral dosing regimen achieved plasma concentrations near or above 1  $\mu$ mol/L (particularly in mouse and dog; Supplementary Fig. S3A, data not shown). Furthermore, this pharmacokinetic analysis demonstrated a half-life predictive of once-daily oral dosing for each agent (or potentially twice daily for GNS-1481 pending ongoing *in vivo* pharmacokinetic assessment; Supplementary Fig. S3A, data not

shown). Importantly, no systemic toxicity was noted in the animals during the pharmacokinetic and dose-finding studies (data not shown).

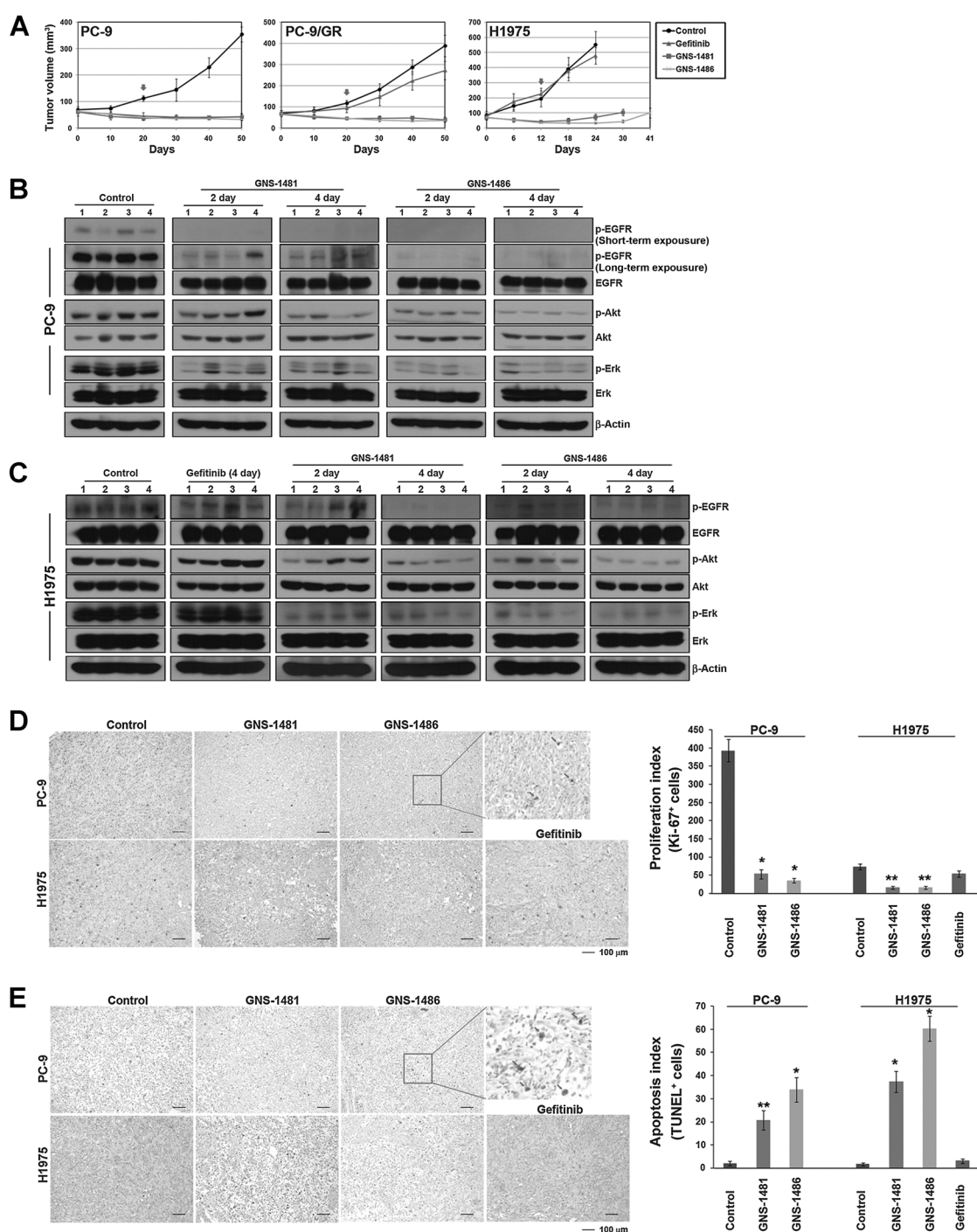
We further tested the efficacy of GNS-1481 and GNS-1486 treatment against multiple human EGFR-mutant lung adenocarcinoma models implanted subcutaneously into mice, including models with EGFR<sup>T790M</sup> (PC-9/GR and H1975; Fig. 4A). We found that once-daily oral treatment with either agent demonstrated substantial *in vivo* efficacy in each model, inducing sustained tumor regressions in PC-9 and PC-9/GR tumors and initial regressions and subsequent disease control in H1975 tumors (Fig. 4A). The efficacy of GNS-1481 and GNS-1486 was similar to gefitinib in the PC9 (EGFR<sup>Del 19</sup>) tumor xenografts, and superior to gefitinib in the PC9/GR (EGFR<sup>Del19/T790M</sup>) and H1975 (EGFR<sup>L858R/T790M</sup>) tumor xenografts, as expected given that gefitinib is largely inactive against EGFR<sup>T790M</sup>-positive cancers (Fig. 4A). The antitumor efficacy of GNS-1481 and GNS-1486 occurred without substantial overt toxicity in the treated animals (Supplementary Fig. S3B, data not shown). Analysis of key pharmacodynamic biomarkers, including p-EGFR, p-AKT, and p-ERK, indicated that GNS-1481 and GNS-1486 substantially suppressed EGFR activation and downstream signaling (Fig. 4B and C). These effects of GNS-1481 and GNS-1486 treatment on signaling were accompanied by decreased proliferation (as measured by quantitative analysis of Ki-67 staining in the tumor cells by IHC) and increased apoptosis (as measured by quantitative analysis of TUNEL staining in the tumor cells by IHC; Fig. 4D and E). Moreover, we compared the activity of the GNS agents with osimertinib in two distinct EGFR<sup>T790M</sup>-positive *in vivo* models and, overall, found comparable antitumor and signaling effects in response to treatment with each drug (Supplementary Fig. S4A–S4D). However, we found that both GNS-1486 and GNS-1481 showed less activity against WT EGFR in the skin of treated animals in multiple different *in vivo* systems, compared with treatment with either erlotinib or osimertinib and at doses where p-EGFR inhibition in the tumors (H1975) *in vivo* was equivalent between the GNS agents and osimertinib (Supplementary Fig. S4E and S4F). Together, these data indicate that GNS-1481 and GNS-1486 show substantial mutant EGFR-selective, oral antitumor efficacy with less activity against WT EGFR *in vivo* than currently approved EGFR TKIs (including osimertinib), offering a potentially wider safety margin than these current EGFR TKIs while showing substantial antitumor efficacy.

#### Intracranial antitumor efficacy of the novel mutant-selective EGFR kinase inhibitor GNS-1486 *in vivo*

During the preclinical pharmacology and pharmacokinetic *in vivo* analysis, we noted that GNS-1481 and GNS-1486 exhibited substantial CNS penetration, with intravenous administration in rats resulting in a CNS/plasma concentration ratio of 0.53–6.15 within 2 hours of initial dosing (Supplementary Table S3). These observations suggested that GNS-1481 or GNS-1486 could potentially show efficacy against intracranial tumors *in vivo*. We tested this hypothesis by establishing intracranial tumors in mice using human EGFR-mutant (Del 19) lung adenocarcinoma cells engineered to stably express a luciferase reporter to enable *in vivo* bioluminescence-based monitoring of tumor growth (HCC827-Luc cells, Fig. 5A). Intracranial implantation of HCC827-Luc cells

resulted in substantial tumor growth in the brain within 2 to 3 weeks, confirmed by both BLI and by pathologic analysis of brain sections obtained from tumor-bearing mice (Fig. 5A and B). We then treated mice with established intracranial EGFR-mutant lung adenocarcinoma with once-daily orally administered GNS-1486 and assessed CNS tumor growth *in vivo*, making comparison with osimertinib as the only approved third-generation EGFR inhibitor and that has shown some CNS activity in limited published reports (30, 31). Importantly, the CNS activity of osimertinib and other EGFR TKIs in patients remains under active clinical investigation and has not yet been firmly established in large patient cohorts (to our knowledge). GNS-1486 was chosen for study because of its better selectivity for mutant EGFR over WT EGFR, and its improved pharmacokinetic parameters compared with GNS-1481. We found that once-daily oral GNS-1486 substantially suppressed intracranial tumor growth in these mice, as measured both by BLI and  $\mu$ CT (Fig. 5C–G). In an animal with a large detectable spinal metastasis, we further noted excellent *in vivo* activity of GNS-1486 against both the primary brain and spinal tumors, consistent with the substantial CNS penetration demonstrated by this agent (Supplementary Fig. S5A). We found that CO-1686 (rociletinib) did not, but osimertinib did show CNS activity in the HCC827 intracranial tumor system (Fig. 6A–D, data not shown), consistent with prior data (30). However, GNS-1486 showed increased potency versus osimertinib against the CNS metastases in this *in vivo* system, as evidenced by the increased efficacy of GNS-1486 versus osimertinib at the 3 mg/kg/day dosing of each agent (measured by quantitative BLI analysis and comparison;  $P = 0.044$  for 3 mg/kg GNS-1486 superiority vs. 3 mg/kg osimertinib at 1 week and  $P = 0.007$  for 3 mg/kg GNS-1486 superiority vs. 3 mg/kg osimertinib at 2 weeks; Figs. 5D–F and 6B–E).

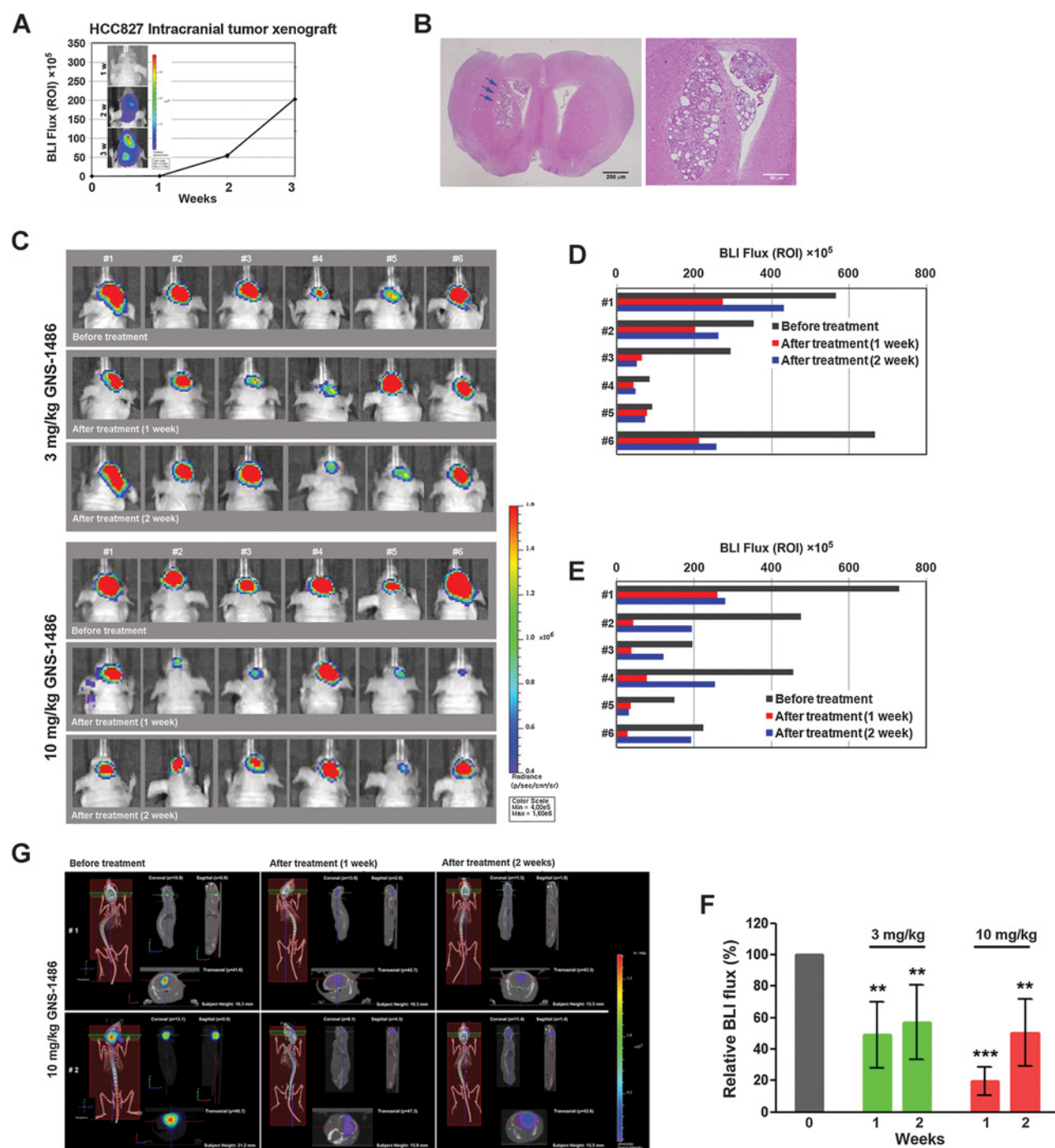
Consistent with these observations, we found that GNS-1486 treatment suppressed p-EGFR, p-AKT, and p-ERK levels and increased apoptosis as measured by both cleaved PARP and caspase-3 levels in the intracranial tumors, again with an improved potency compared with osimertinib as shown by the increased efficacy of GNS-1486 versus osimertinib in the 3 mg/kg/day treatment cohorts [p-EGFR:  $P < 0.0001$  for 3 mg/kg GNS-1486 superiority vs. 3 mg/kg osimertinib; p-Akt:  $P = 0.004$  for 3 mg/kg GNS-1486 superiority vs. 3 mg/kg osimertinib; p-Erk:  $P = 0.015$  for 3 mg/kg GNS-1486 superiority vs. 3 mg/kg osimertinib; cleaved PARP:  $P = 0.028$  for 3 mg/kg GNS-1486 superiority vs. 3 mg/kg osimertinib; cleaved caspase-3:  $P = 0.018$  for 3 mg/kg GNS-1486 superiority vs. 3 mg/kg osimertinib (Supplementary Fig. S5B)]. Superior *in vivo* pharmacodynamics of GNS-1486 versus osimertinib were also observed at the higher 10 mg/kg/day cohorts for certain pharmacodynamic biomarkers (p-Erk:  $P = 0.049$  for 10 mg/kg GNS-1486 superiority vs. 10 mg/kg osimertinib; cleaved PARP:  $P = 0.016$  for 10 mg/kg GNS-1486 superiority vs. 10 mg/kg osimertinib; cleaved caspase-3:  $P = 0.024$  for 10 mg/kg GNS-1486 superiority vs. 10 mg/kg osimertinib; p-EGFR:  $P = 0.16$  for 10 mg/kg GNS-1486 vs. 10 mg/kg osimertinib; p-Akt:  $P = 0.334$  for 10 mg/kg GNS-1486 vs. 10 mg/kg osimertinib); in contrast to the 3 mg/kg/day comparison between GNS-1486 and osimertinib, these improved pharmacodynamic effects at the 10 mg/kg dose were not associated with statistically significant differences in the antitumor efficacy as measured by BLI analysis at these higher drug doses and time points in

**Figure 4.**

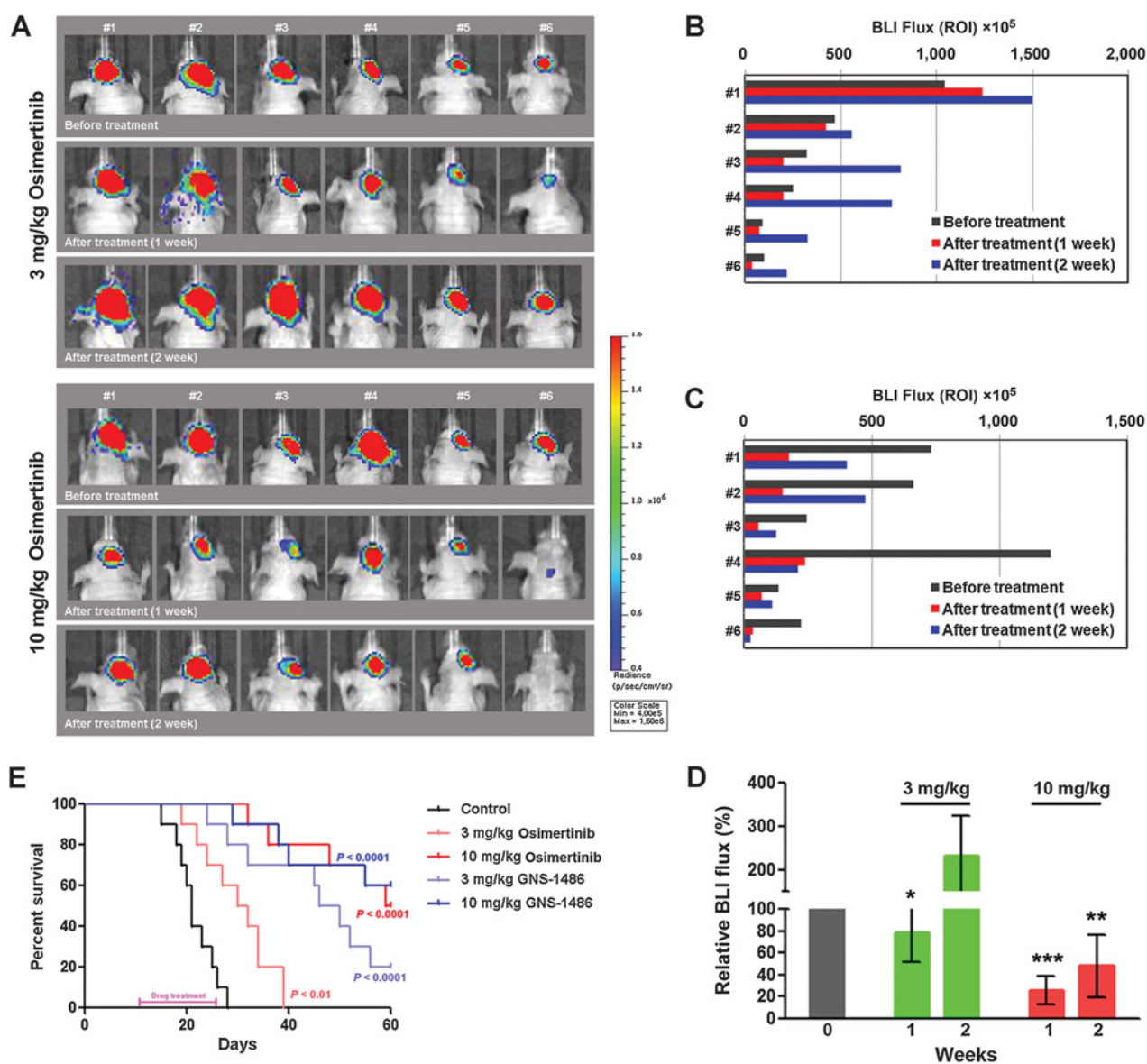
Preclinical efficacy of the novel mutant-selective EGFR kinase inhibitors GNS-1481 and GNS-1486 *in vivo*. **A**, *In vivo* antitumor efficacy of the indicated EGFR inhibitors in the subcutaneous tumor xenografts in mice ( $n = 5$  per treatment cohort for each xenograft model). Mice were treated orally with vehicle or 30 mg/kg/day GNS-1481 or GNS-1486 or 100 mg/kg/day of gefitinib daily (5 consecutive days/week). Results are shown as tumor volume measurements over the time course of treatment with vehicle control or each EGFR inhibitor and presented as  $\pm$ SEM. Each treatment was initiated at day 0, and the arrow indicates cessation of each therapy, with continued measurement of tumor volumes to the endpoint. **B** and **C**, Immunoblot analysis measuring each indicated pharmacodynamic biomarker in representative control-treated or EGFR inhibitor-treated tumors harvested from tumor-bearing mice at the indicated time points following the initiation of therapy. **B**, The analysis of PC-9 tumors. **C**, The analysis of H1975 tumors. Results represent at least three independent experiments. **D** and **E**, Immunohistochemical analysis measuring each indicated pharmacodynamic biomarker (**D**, Ki-67; **E**, TUNEL staining) in representative control-treated or EGFR inhibitor-treated tumors harvested from tumor-bearing mice at 4 days following the initiation of therapy. Inset on the right shows quantification of the Ki-67 and TUNEL staining in **D** and **E** under each condition. \*,  $P < 0.01$ ; \*\*,  $P < 0.001$  for GNS-1481 or GNS-1486 versus control (vehicle-treated) tumors.



Rho et al.

**Figure 5.**

Intracranial antitumor efficacy of the novel mutant-selective EGFR kinase inhibitor GNS-1486 *in vivo*. **A**, Establishment of the EGFR-mutant lung adenocarcinoma intracranial model using HCC827 cells stably expressing the luciferase reporter (HCC827-Luc). BLI was used to detect and monitor intracranial tumor growth *in vivo*. Shown is a representative mouse with intracranial tumor growth within 3 weeks following intracranial implantation. **B**, Histologic analysis of HCC827-Luc tumor in a representative mouse following intracranial implantation. Hematoxylin and eosin staining of tumor sections obtained following intracranial tumor harvest from an individual mouse shows lung adenocarcinoma formation in the brain. Arrows, areas of tumor in the brain parenchyma. **C–G**, BLI  $\mu$ CT images and quantification analysis of intracranial HCC827-Luc tumor growth before and during oral treatment with GNS-1486 (5 consecutive days/week,  $n = 6$  animals) at the indicated time points and drug doses. Red pseudocoloring indicates increased tumor growth and green-blue pseudocoloring indicates decreased tumor growth by bioluminescence quantification in **C** and **G**. **D–F**, Quantification of the bioluminescence photon flux in the mice with intracranial HCC827-Luc tumors treated over the indicated time points. \*\*,  $P < 0.001$ ; \*\*\*,  $P < 0.0001$  for drug versus control (vehicle-treated) tumors. For all treatment studies, baseline imaging and subsequent therapy was initiated 14 days following intracranial tumor cell implantation.

**Figure 6.**

Intracranial antitumor efficacy of GNS-1486 and osimertinib *in vivo*. **A–D**, BLI  $\mu$ CT images and quantification analysis of intracranial HCC827-Luc tumor growth before and during oral treatment with osimertinib (5 consecutive days/week,  $n = 6$  animals) at the indicated time points and drug doses. Red pseudocoloring indicates increased tumor growth and green-blue pseudo-coloring indicates decreased tumor growth by bioluminescence quantification in **A**. **B–D**, Quantification of the bioluminescence photon flux in the mice with intracranial HCC827-Luc tumors treated over the indicated time points. \*,  $P < 0.01$  and \*\*,  $P < 0.001$ ; \*\*\*,  $P < 0.0001$  for drug versus control (vehicle treated) tumors. **E**, Kaplan-Meier survival curves of HCC827-Luc cell line in mice treated with the indicated oral doses of either GNS-1486 or AZD9291 daily for 2 weeks, indicated by the purple line on the x-axis ( $n = 7$  animals per cohort;  $P$  values shown compared with control treatment). For all treatment studies, baseline imaging and subsequent therapy was initiated 14 days following intracranial tumor cell implantation.

this system ( $P = 0.28$  for 10 mg/kg GNS-1486 vs. 10 mg/kg osimertinib at 1 week;  $P = 0.9$  for 10 mg/kg GNS-1486 vs. 10 mg/kg osimertinib at 2 weeks; Figs. 5D–F and 6B–D).

We further found that treatment with GNS-1486 substantially improved survival in mice with intracranial EGFR-mutant tumors (using the HCC827-Luc system; Fig. 6E). We again noted an improved potency of GNS-1486 compared with osimertinib in these preclinical trials, as evidenced by the efficacy outcome data in the 3 mg/kg/day treatment cohorts ( $P = 0.0035$  for 3

mg/kg GNS-1486 superiority vs. 3 mg/kg osimertinib;  $P = 0.7519$  for 10 mg/kg GNS-1486 vs. 10 mg/kg osimertinib). We further confirmed the substantial intracranial antitumor activity of GNS-1486 in an additional patient-derived EGFR-mutant lung adenocarcinoma model (H1975 EGFR<sup>L858R/T790M</sup> cells; Supplementary Fig. S6). In contrast, CO-1686 (rociletinib) treatment was less effective in this intracranial H1975 tumor system (Supplementary Fig. S6). Importantly, no signs of systemic or CNS toxicity were noted during treatment with GNS-1486 in the mice (data not

shown), consistent with the high selectivity for mutant EGFR versus WT EGFR we observed for this agent. The data suggest that GNS-1486 exhibits superior potency against EGFR-mutant lung adenocarcinoma CNS disease versus osimertinib (and rociletinib) in these *in vivo* systems, offering a new highly effective therapeutic agent whose potency and selectivity for mutant EGFR provides the potential advantage of decreased clinical toxicity. Altogether, these findings establish GNS-1486 as a novel, improved, orally administered, CNS-penetrant, and mutant-selective EGFR (including EGFR<sup>T790M</sup>) inhibitor with both potent extracranial and intracranial antitumor efficacy and a wide apparent safety margin. The data provide the rationale for clinical trials, testing the safety and efficacy of GNS-1486 in EGFR-mutant (including EGFR<sup>T790M</sup>) lung adenocarcinoma patients with active CNS metastatic disease (as well as extracranial disease); these trials will be initiated soon.

## Discussion

In summary, despite recent important progress in the field, the identification of a potent, more mutant EGFR-selective and CNS-active EGFR TKI with an improved safety margin could have a substantial and immediate beneficial impact on both patient outcomes and quality of life. Toward this end, our study establishes the preclinical efficacy, safety, and potential clinical utility of novel mutant-selective EGFR TKIs (GNS-1481, GNS-1486). The improved, potent mutant-EGFR selective agents that we describe here show two important advantages over the currently approved EGFR TKIs, including osimertinib: (i) less WT EGFR inhibition and, therefore, risk of toxicity while exhibiting substantial antitumor efficacy and (ii) improved potency against CNS metastasis. Given these distinct attributes, these new EGFR TKIs complement the currently approved EGFR TKIs and are now under clinical development; indeed, clinical trials testing these new agents in EGFR-mutant (including EGFR<sup>T790M</sup>) lung adenocarcinoma patients with active CNS and extracranial metastatic disease will be initiated soon. Although only these clinical trials can establish whether the greater selectivity for mutant EGFR versus WT EGFR and the increased potency against CNS disease that we observed in the preclinical systems will yield improved outcomes and safety in patients, these promising new agents have the potential to exhibit efficacy in patients with both extracranial and intracranial EGFR-mutant lung adenocarcinoma (including EGFR<sup>T790M</sup>-positive disease), with less clinical toxicity, to thereby potentially improve not only the quantity but also quality of life for patients. Our study highlights the utility of identifying

highly potent and oncoprotein-selective targeted agents that show substantial activity against CNS metastasis early in the drug discovery and development process to reduce both clinical toxicity and the high burden and related mortality of CNS metastasis, as well as extracranial disease, in patients.

## Disclosure of Potential Conflicts of Interest

T.G. Bivona reports receiving other commercial research support from Ignyta and is a consultant/advisory board member for Array, AstraZeneca, and Novartis. No potential conflicts of interest were disclosed by the other authors.

## Authors' Contributions

**Conception and design:** J.K. Rho, I.Y. Lee, C.-M. Choi, J.S. Koh, J. Lee, H.-J. Song, P. Salgaonkar, Jaesang Lee, W.S. Kim, C.H. Kim, T.G. Bivona, J.C. Lee

**Development of methodology:** I.Y. Lee, B.-C. Suh, H.-J. Song, Jaesang Lee, D.S. Jung, D.-C. Woo, I.-J. Baek, J.-Y. Lee, J.K. Kim

**Acquisition of data (provided animals, acquired and managed patients, provided facilities, etc.):** J.K. Rho, I.Y. Lee, C.-M. Choi, J.-Y. Hur, B.-C. Suh, H.-J. Song, P. Salgaonkar, Jaesang Lee, D.S. Jung, S.-Y. Kim, I.-J. Baek, Y.H. Sung, J.K. Kim, W.S. Kim, J.S. Song

**Analysis and interpretation of data (e.g., statistical analysis, biostatistics, computational analysis):** J.K. Rho, I.Y. Lee, Y.J. Choi, B.-C. Suh, H.-J. Song, Jungmi Lee, Jaesang Lee, D.S. Jung, D.-C. Woo, C.H. Ha, J.K. Kim, C.H. Kim, T.G. Bivona, J.C. Lee

**Writing, review, and/or revision of the manuscript:** J.K. Rho, I.Y. Lee, B.-C. Suh, H.-J. Song, P. Salgaonkar, Jaesang Lee, J.K. Kim, T.G. Bivona, J.C. Lee

**Administrative, technical, or material support (i.e., reporting or organizing data, constructing databases):** J.K. Rho, I.Y. Lee, J.K. Kim, C.H. Kim, T.G. Bivona, J.C. Lee

**Study supervision:** J.K. Rho, C.-M. Choi, H.-J. Song, P. Salgaonkar, J.K. Kim, C.H. Kim, T.G. Bivona, J.C. Lee

**Other (synthesis of small-molecule kinase inhibitors being tested in this study):** P. Salgaonkar

## Grant Support

This study was supported by the Basic Science Research Program through the National Research Foundation of Korea (NRF, grant 2013R1A1A2005112 to J.K. Rho and grant 2014R1A2A2A01003438 to J.C. Lee) and a grant of the Korea Health Technology R&D Project through the Korea Health Industry Development Institute (KHIDI), funded by the Ministry of Health & Welfare, Republic of Korea (grant HI15C0516). T.G. Bivona acknowledges support from NIH (NIH Director's New Innovator Award, grants DP2 CA174497 and R01 CA169338).

The costs of publication of this article were defrayed in part by the payment of page charges. This article must therefore be hereby marked *advertisement* in accordance with 18 U.S.C. Section 1734 solely to indicate this fact.

Received September 7, 2016; revised November 15, 2016; accepted December 7, 2016; published OnlineFirst January 12, 2017.

## References

1. The Cancer Genome Atlas Research Network. Comprehensive molecular profiling of lung adenocarcinoma. *Nature* 2014;511:543–50.
2. Swanton C, Govindan R. Clinical implications of genomic discoveries in lung cancer. *N Engl J Med* 2016;374:1864–73.
3. Lynch TJ, Bell DW, Sordella R, Curubhagavatula S, Okimoto RA, Brannigan BW, et al. Activating mutations in the epidermal growth factor receptor underlying responsiveness of non-small-cell lung cancer to gefitinib. *N Engl J Med* 2004;350:2129–39.
4. Pao W, Miller V, Zakowski M, Doherty J, Politi K, Sarkaria I, et al. EGF receptor gene mutations are common in lung cancers from "never smokers" and are associated with sensitivity of tumors to gefitinib and erlotinib. *Proc Natl Acad Sci U S A* 2004;101:13306–11.
5. Paez JG, Jänne PA, Lee JC, Tracy S, Greulich H, Gabriel S, et al. EGFR mutations in lung cancer: correlation with clinical response to gefitinib therapy. *Science* 2004;304:1497–500.
6. Rosell R, Moran T, Queralt C, Porta R, Cardenal F, Camps C, et al. Screening for epidermal growth factor receptor mutations in lung cancer. *N Engl J Med* 2009;361:958–67.
7. Mok TS, Wu YL, Thongprasert S, Yang CH, Chu DT, Saijo N, et al. Gefitinib or carboplatin-paclitaxel in pulmonary adenocarcinoma. *N Engl J Med* 2009;361:947–57.
8. Soda M, Choi YL, Enomoto M, Takada S, Yamashita Y, Ishikawa S, et al. Identification of the transforming EML4-ALK fusion gene in non-small-cell lung cancer. *Nature* 2007;448:561–6.

9. Shaw AT, Kim D-W, Nakagawa K, Seto T, Crinó L, Ahn M-J, et al. Crizotinib versus chemotherapy in advanced ALK-positive lung cancer. *N Engl J Med* 2013;368:2385–94.
10. Rosell R, Bivona TG, Karachaliou N. Genetics and biomarkers in personalisation of lung cancer treatment. *Lancet* 2013;382:720–31.
11. Bivona TG, Doebele RC. A framework for understanding and targeting residual disease in oncogene-driven solid cancers. *Nat Med* 2016;22:472–8.
12. Politi K, Ayeni D, Lynch T. The next wave of EGFR tyrosine kinase inhibitors enter the clinic. *Cancer Cell* 2015;27:751–3.
13. Garraway LA, Janne PA. Circumventing cancer drug resistance in the era of personalized medicine. *Cancer Discov* 2012;2:214–26.
14. Sawyers CL. The 2011 Gordon Wilson Lecture: overcoming resistance to targeted cancer drugs. *Trans Am Clin Climatol Assoc* 2012;123:114–23.
15. Pazarentzos E, Bivona TG. Adaptive stress signaling in targeted cancer therapy resistance. *Oncogene* 2015;34:5599–606.
16. Bivona TG, Hieronymus H, Parker J, Chang K, Taron M, Rosell R, et al. FAS and NF-kappaB signalling modulate dependence of lung cancers on mutant EGFR. *Nature* 2011;471:523–6.
17. Crystal AS, Shaw AT, Sequist LV, Friboulet L, Niederst MJ, Lockerman EL, et al. Patient-derived models of acquired resistance can identify effective drug combinations for cancer. *Science* 2014;346:1480–6.
18. Hrustanovic G, Olivas V, Pazarentzos E, Tulpule A, Asthana S, Blakely CM, et al. RAS-MAPK dependence underlies a rational polytherapy strategy in EML4-ALK-positive lung cancer. *Nat Med* 2015;21:1038–47.
19. Owonikoko TK, Arbiser J, Zelnak A, Shu HK, Shim H, Robin AM, et al. Current approaches to the treatment of metastatic brain tumours. *Nat Rev Clin Oncol* 2014;11:203–22.
20. Ali A, Goffin JR, Arnold A, Ellis PM. Survival of patients with non-small-cell lung cancer after a diagnosis of brain metastases. *Curr Oncol* 2013;20:e300–6.
21. Camidge DR, Pao W, Sequist LV. Acquired resistance to TKIs in solid tumours: learning from lung cancer. *Nat Rev Clin Oncol* 2014;11:473–81.
22. Yu HA, Arcila ME, Rekhman N, Sima CS, Zakowski MF, Pao W, et al. Analysis of tumor specimens at the time of acquired resistance to EGFR-TKI therapy in 155 patients with EGFR-mutant lung cancers. *Clin Cancer Res* 2013;19:2240–7.
23. Walter AO, Sjin RT, Haringsma HJ, Ohashi K, Sun J, Lee K, et al. Discovery of a mutant-selective covalent inhibitor of EGFR that overcomes T790M-mediated resistance in NSCLC. *Cancer Discov* 2013;3:1404–15.
24. Cross DA, Ashton SE, Ghiorghiu S, Eberlein C, Nebhan CA, Spitzler PJ, et al. AZD9291, an irreversible EGFR TKI, overcomes T790M-mediated resistance to EGFR inhibitors in lung cancer. *Cancer Discov* 2014;4:1046–61.
25. Sequist LV, Rolfe L, Allen AR. Rociletinib in EGFR-mutated non-small-cell lung cancer. *N Engl J Med* 2015;372:1700–9.
26. Janne PA, Yang JC-H, Kim D-W, Planchard D, Ohe Y, Ramalingam SS, et al. AZD9291 in EGFR inhibitor-resistant non-small-cell lung cancer. *N Engl J Med* 2015;372:1689–99.
27. Thress KS, Paweletz CP, Felip E, Cho BC, Stetson D, Dougherty B, et al. Acquired EGFR C797S mutation mediates resistance to AZD9291 in non-small cell lung cancer harboring EGFR T790M. *Nat Med* 2015;21:560–2.
28. Piotrowska Z, Niederst MJ, Karlovich CA, Wakelee HA, Neal JW, Mino-Kenudson M, et al. Heterogeneity underlies the emergence of EGFR T790 wild-type clones following treatment of T790M-positive cancers with a third generation EGFR inhibitor. *Cancer Discov* 2015;5:713–22.
29. Lin L, Bivona TG. Mechanisms of resistance to epidermal growth factor receptor inhibitors and novel therapeutic strategies to overcome resistance in NSCLC patients. *Chemother Res Pract* 2012;2012:817297.
30. Ballard P, Yates JW, Yang Z, Kim DW, Yang JC, Cantarini M, et al. Preclinical comparison of osimertinib with other EGFR-TKIs in EGFR-Mutant NSCLC brain metastases models, and early evidence of clinical brain metastases activity. *Clin Cancer Res* 2016;22:5130–40.
31. Ricciuti B, Chiari R, Chiarini P, Crinó L, Maletini D, Ludovini V, et al. Osimertinib (AZD9291) and CNS response in two radiotherapy-naive patients with EGFR-mutant and T790M-positive advanced non-small cell lung cancer. *Clin Drug Investig* 2016;36:683–6.
32. Yu HA, Tian SK, Drilon AE, Borsu L, Riely GJ, Arcila ME, et al. Acquired resistance of EGFR-mutant lung cancer to a T790M-specific EGFR inhibitor: emergence of a third mutation (C797S) in the EGFR tyrosine kinase domain. *JAMA Oncol* 2015;1:982–4.
33. Rho JK, Choi YJ, Lee JK, Ryoo BY, Na II, Yang SH, et al. The role of MET activation in determining the sensitivity to epidermal growth factor receptor tyrosine kinase inhibitors. *Mol Cancer Res* 2009;7:1736–43.
34. Carlomagno F, Guida T, Anaganti S, Vecchio G, Fusco A, Ryan AJ, et al. Disease associated mutations at valine 804 in the RET receptor tyrosine kinase confer resistance to selective kinase inhibitors. *Oncogene* 2004;23:6056–63.
35. Takeuchi K, Soda M, Togashi Y, Suzuki R, Sakata S, Hatano S, et al. RET, ROS1 and ALK fusions in lung cancer. *Nat Med* 2012;18:378–81.
36. Marusiak AA, Edwards ZC, Hugo W, Trotter EW, Girotti MR, Stephenson NL, et al. Mixed lineage kinases activate MEK independently of RAF to mediate resistance to RAF inhibitors. *Nat Commun* 2014;5:3901.
37. Tricker EM, Xu C, Uddin S, Capelletti M, Ercan D, Ogino A, et al. Combined EGFR/MEK inhibition prevents the emergence of resistance in EGFR-mutant lung cancer. *Cancer Discov* 2015;5:960–71.
38. Rho JK, Choi YJ, Jeon BS, Choi SJ, Cheon GJ, Woo SK, et al. Combined treatment with silibinin and epidermal growth factor receptor tyrosine kinase inhibitors overcomes drug resistance caused by T790M mutation. *Mol Cancer Ther* 2010;9:3233–43.
39. Zhang Z, Lee JC, Lin L, Olivas V, Au V, LaFramboise T, et al. Activation of the AXL kinase causes resistance to EGFR-targeted therapy in lung cancer. *Nat Genet* 2012;44:852–60.
40. Rho JK, Choi YJ, Kim SY, Kim TW, Choi EK, Yoon SJ, et al. MET and AXL inhibitor NPS-1034 exerts efficacy against lung cancer cells resistant to EGFR kinase inhibitors because of MET or AXL activation. *Cancer Res* 2014;74:253–62.

# Cancer Research

The Journal of Cancer Research (1916–1930) | The American Journal of Cancer (1931–1940)

## Superior Efficacy and Selectivity of Novel Small-Molecule Kinase Inhibitors of T790M-Mutant EGFR in Preclinical Models of Lung Cancer

Jin Kyung Rho, In Yong Lee, Yun Jung Choi, et al.

*Cancer Res* 2017;77:1200-1211. Published OnlineFirst January 12, 2017.

|                               |   |
|-------------------------------|---|
| <b>Updated version</b>        | Access the most recent version of this article at:<br>doi: <a href="https://doi.org/10.1158/0008-5472.CAN-16-2432">10.1158/0008-5472.CAN-16-2432</a>  |
| <b>Supplementary Material</b> | Access the most recent supplemental material at:<br><a href="http://cancerres.aacrjournals.org/content/suppl/2017/01/12/0008-5472.CAN-16-2432.DC1">http://cancerres.aacrjournals.org/content/suppl/2017/01/12/0008-5472.CAN-16-2432.DC1</a> |

|                        |   |
|------------------------|---|
| <b>Cited articles</b>  | This article cites 40 articles, 13 of which you can access for free at:<br><a href="http://cancerres.aacrjournals.org/content/77/5/1200.full#ref-list-1">http://cancerres.aacrjournals.org/content/77/5/1200.full#ref-list-1</a>                |
| <b>Citing articles</b> | This article has been cited by 1 HighWire-hosted articles. Access the articles at:<br><a href="http://cancerres.aacrjournals.org/content/77/5/1200.full#related-urls">http://cancerres.aacrjournals.org/content/77/5/1200.full#related-urls</a> |

|                                   |  |
|-----------------------------------|--|
| <b>E-mail alerts</b>              | <a href="#">Sign up to receive free email-alerts</a> related to this article or journal.   |
| <b>Reprints and Subscriptions</b> | To order reprints of this article or to subscribe to the journal, contact the AACR Publications Department at <a href="mailto:pubs@aacr.org">pubs@aacr.org</a> .   |
| <b>Permissions</b>                | To request permission to re-use all or part of this article, use this link<br><a href="http://cancerres.aacrjournals.org/content/77/5/1200">http://cancerres.aacrjournals.org/content/77/5/1200</a> .<br>Click on "Request Permissions" which will take you to the Copyright Clearance Center's (CCC) Rightslink site. |